Conductive ZSM-5-Based Adsorbent for CO2 Capture: Active Phase vs Monolith

Published version:

DOI:10.1021/acs.iecr.7b01058

Alessio Masala, Jenny G. Vitillo, Giorgia Mondino, Gianmario Martra, Richard Blom, Carlos A. Grande, Silvia Bordiga

Paper: Conductive ZSM-5-Based Adsorbent for CO2 Capture: Active Phase vs Monolith

INDUSTRIAL & ENGINEERING CHEMISTRY RESEARCH, 56 (30), 2017, pp: 8485–8498
DOI: 10.1021/acs.iecr.7b01058

Conductive ZSM-5-based adsorbent for CO_2 capture: active phase vs. monolith

Alessio Masala[†‡], Jenny G. Vitillo[†‡*], Giorgia Mondino[§], Gianmario Martra,[†] Richard Blom,[§] Carlos A. Grande[§] and Silvia Bordiga[†]

[†] Department of Chemistry, NIS and INSTM Reference Centre, University of Turin, Via Quarello 15, 10135 Torino, Italy.

[§] SINTEF Materials and Chemistry, P.O. Box 124 Blindern, N0314 Oslo, Norway.

[‡] The two authors have equally contributed to the manuscript

ABSTRACT. Among microporous adsorbents, zeolites constitute the reference materials in CO_2-capture technologies, because of their high CO_2 affinity, high chemical and thermal stability and their low cost. Being synthetized in powder form, they need to be shaped in pellets or monolith before to be suitable for real applications. The process has a direct effect on CO_2-capture properties of the material creating – in this sense – substantial differences between lab-scale (adsorbents) and plant-scale systems (adsorbers). The ability of the honeycomb monolith to efficiently separate gases of interest, arises from the properties of its single components such as an active phase and a phase resulting from the decomposition of a binder. Moreover, the textural (i.e. pore distribution and exposed surface) and structural properties (e.g. amorphization) of the active phase can be modified in the conditions adopted during the process that leads to the final artifact. These modifications can affect the CO_2-capture performances of the active phase. Nevertheless, often a comparison between the active phase and its corresponding monolith is not possible. In this article, the process to obtain a zeolite/electrical conductive carbon monolith suitable for electric swing adsorption (ESA) process is described. The CO_2 adsorption properties of a zeolite (H-ZSM-5) in powder form and its related shaped monolith have been compared to the uptake of other competitive gases (H_2O, O_2 and N_2). The difference in the adsorption properties between the powder and the monolith have been analyzed by means of volumetric, spectroscopic, diffractometric and microscopic techniques. This study underlined the gap between the CO_2-capture performances of pure active phases – usually studied at the lab scale – and their related final artifacts, instead conceived for industrial applications. Interestingly, in the present case, the extrusion of a monolith composed by an active phase and a conductive phase had three positive effects (besides those expected) with respect to the pristine powder: (i) increase in the heat capacity of the material; (ii) decrease the water heat of adsorption; (iii) increase in the CO_2 isosteric heat of adsorption. Whereas the first point is easily correlated to the carbonaceous phase present in the composite, the third can be related to the partial H^+/Na^+ exchange occurring along with the monolith preparation, as identified by infrared (IR) and energy dispersive X-Ray spectroscopies (EDS). The increase in the hydrophobicity of the monolith was on the contrary related to both these factors.

1. Introduction

Carbon dioxide capture in post-combustion energy schemes is nowadays considered one of the most viable ways to decarbonize power generation in the short-medium term.[1-4] The advantage of post-combustion CO_2 capture relies on the possibility to retro-fit this technology to already existing power plants.[3] The state-of-the-art for CO_2 capture from post-combustion flue gases is a process based on chemical fixation by aqueous alkanolamine solutions, normally termed as amine scrubbing. This process is however characterized by regeneration-costs issues.[5] Adsorption potentially ensures a weaker bonding between CO_2 and porous solids than the one usually detected for amine-scrubbing process:[6, 7] the energy penalty related to the CO_2-capture process can be minimized when the CO_2 energy of adsorption reaches an optimal value, as demonstrated by Pirngruber, Smit and Sholl.[8-10] Moreover, typical properties of solid adsorbents – zeolites, active carbons or the new generation metal-organic frameworks – such as a low heat capacity (important for temperature swing adsorption, TSA)[3, 11, 12] and a low-medium strength interaction with CO_2,[13-15] offer the possibility to reduce the energetic cost of the recovery step.[6, 16]

However, the implementation of carbon capture technology on a large scale industrial facility requires a series of engineering features that have to be taken into account when designing the solid adsorbent to be coupled with a CO_2–capture unit. In fact, the use of adsorbents – usually microporous materials with high affinity for CO_2 – in their granular/powder state often implies poor adsorption per unit volume, large pressure drops[17-19] and low thermal conductivity along the fixed-bed length, leading to strong decreases in the uptake capacity (up to 50%).[20] The employment of an adsorbent with the proper shape can affect positively on the above mentioned drawbacks and so on the costs related to the entire process.[18]

Monolithic adsorbents are among the new structured materials – together with fabric structures, foams or laminates – that encountered the attention of the scientific community for gas adsorption, during the last decades.[21-26] They can be characterized by different shapes such as cylindrical, flat plates or block shaped,[1, 27-29] although the honeycomb topology is the one that guarantees the smallest pressure drop thanks to the presence of straight parallel channels extending along the composite body.[21, 25]

Among post-combustion carbon capture, electric swing adsorption (ESA) is a process in which the recovery of the adsorbent is obtained by passing electricity through the material, consequentially heated up by means of Joule effect.[21] ESA process can be more effective than TSA if the adsorbent itself is a good electric conductor (e.g. graphitic carbons).[2] In order to obtain a conductive carbon monolith, the easiest and most effective procedure is to prepare a heterogeneous mixture of an active phase and a binder resin and extrude the mixture at high temperatures to give – together with mechanical strength – conductive properties to the final artifact.[1, 17] The production of a monolith is nowadays mainly conducted by the above-cited extrusion method, even though recent works demonstrated the validity of 3D-printing as reliable tool to create structured adsorbents with precise geometries, also at the lab scale.[30, 31] Binder and active phase portions must be carefully chosen because the presence of the former (inert binder) can decrease the efficiency in CO_2 uptake, inducing a gap in the performances of the monolithic adsorbent and the pure active phase. Moreover, the high temperature used for the carbonization of the binder can drastically affect the structure of the active phase. Pore blocking in the active phase due to partial adsorption of the binder could be also not negligible. Because of the different technological readiness levels of a monolith and its corresponding active phase, a comparison among the two is not often possible.

The present work reports the performance of a zeolitic active phase (a protonic ZSM-5, MFI framework) and its related monolithic form (78 wt.% H-ZSM-5 / 22 wt.% phenolic resin), to be employed for post-combustion carbon capture. The monolith synthesis occurred at high temperature (800 °C) in order to convert the phenolic resin into a conductive carbon phase. Three samples were considered: the monolith, a powder H-ZSM-5 sample previously subjected to a temperature treatment of 800 °C (H-ZSM-5-800) as in the monolith synthesis and a powder H-ZSM-5 sample that was subjected to the lowest treatment temperature sufficient to remove all the water molecules, that is the one that would be used typically in an academic study on the pure active phase (500°C, H-ZSM-5-500). A multi-technique approach has been adopted in this work in order to cover the most relevant properties of these systems: the structural/compositional properties of both the zeolites and the carbon monolith were evaluated by means of powder X-ray diffraction (P-XRD), surface area analysis, Fourier-transformed infrared spectroscopy (FTIR) and transmission electron microscopy (TEM) coupled with energy dispersive spectroscopy (EDS). Thermal characteristics have been also checked through thermal gravimetric analysis (TGA) and differential scanning calorimetry (DSC).

To this set of characterization techniques, the measure of adsorption equilibrium and diffusion of CO_2, N_2, and O_2 at different temperatures was done. The selectivity factors were calculated by exploiting the Ideal Adsorbed Solution Theory (IAST) for a CO_2/N_2 mixture in presence of 5 vol.% O_2 to elucidate the CO_2 separation character of H-ZSM-5 and its related monolith. The isosteric heat of adsorption for CO_2, N_2 and O_2 was also evaluated through the analysis of the volumetric isotherms. Water adsorption isotherms were also obtained by means of microgravimetry and the adsorption heat was evaluated by means of microcalorimetry.

2. Materials and Methods

2.1 Materials

H-ZSM-5-500. H-ZSM-5 sample was obtained by using as precursor the corresponding ammonium form (NH_4-ZSM-5, Zeolyst, the Netherlands, product CBV3024E, SiO_2/Al_2O_3 = 30, Na_2O 0.05 wt.%, SA 405 $m^2\ g^{-1}$) by heating the zeolite in a tubular furnace up to 500°C in N_2 flow (200 ml min^{-1}, ramp rate: 2 °C min^{-1}). The zeolite was kept in isothermal conditions at 500 °C for 2 h, and then cooled down to RT with a ramp rate of 3 °C min^{-1}.

H-ZSM-5-800. H-ZSM-5 sample was obtained by following the same procedure adopted for H-ZSM-5-500, but treating the zeolite at the higher temperature of 800°C, to simulate the conditions encountered by the zeolite in the monolith preparation.

Monolith. NH_4-ZSM-5 precursor was mixed with a phenolic resin (99.5 wt.% in phenol, CAS nr. 28064-14-4, Veritas House, Mumbai, India) and subjected to the conventional process given in Scheme 1. During this process, ammonia evolves with temperature and the precursor NH_4-ZSM-

5 is transformed in the protonic zeolite H-ZSM-5. The final monolith consisted in 78 wt.% of H-ZSM-5 and 22 wt.% of conductive carbon. The monolith was characterized by a conductivity of 29 Ω at RT (measured by a multimeter on a 20 cm monolith).

The process used to fabricate the monoliths is derived from the extrusion process used for ceramic honeycombs developed as catalyst support for automotive exhaust after treatment systems. Cordierite ceramic honeycombs – together with the extrusion process to mass produce them – have been invented in the mid 1970’s to be used as catalytic converters.[32-34]

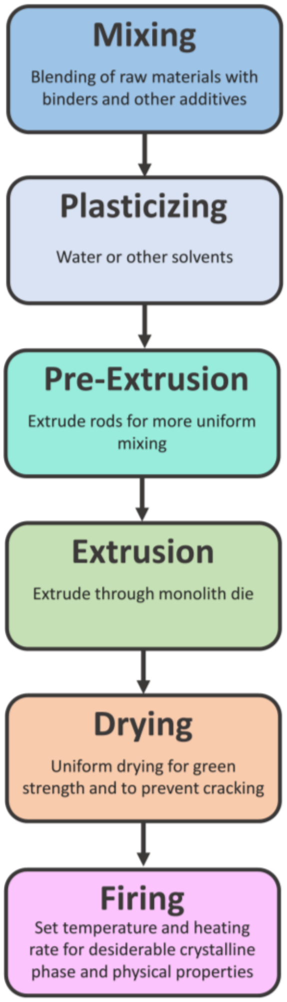

Scheme 1. Conventional process for preparation of extruded ceramic honeycomb monoliths.[35]

In our case, the slight difference from ceramic honeycombs is that the final firing step is here replaced by a carbonization heat treatment to convert the phenolic resin into carbon. The carbonization temperature is set in a manner that the high surface area of the zeolite is preserved while insuring enough conversion into carbon to obtain the desired electrical conductivity. In this case, ZSM-5 zeolite – which demonstrated a high thermal stability in a preliminary characterization – has been subjected to a carbonization treatment of 800°C in order to achieve a full conversion of the resin into a conductive carbon phase.

Carbon(M). The pure carbonaceous part of the monolith was obtained by dissolving the monolith in HF to remove the zeolitic part. The undissolved portion was rinsed three times with distilled water before use.

2.2 Methods

*FTIR spectroscopy***.** In situ FTIR spectra in transmission mode (2 cm^{-1} resolution, average on 32 scans) were collected on a Bruker Vertex70 spectrophotometer. The samples were measured in the form of self-supporting pellets inside a quartz cell in controlled atmosphere. Before each measurement the samples were degassed up to 400°C on a vacuum line equipped with a turbomolecular pump ($< 10^{-4}$ mbar). For what concerns the monolith, an aliquot of the powdered monolith was pressed to form a self-supporting pellet. The pellet was then oxidized in 133 mbar of pure O_2 (3 times, 30 min each time) at 500°C and then degassed under dynamic vacuum (residual pressure: 1.0×10^{-5} mbar) at 500°C for 1 h. The integration of the IR peak was performed by fitting each band by using the *Curve fit* utility of OPUS 5.0 program (Bruker Optic Gmbh), and by integrating the area by using the *Integration* utility of the same program.

Volumetry. N_2, CO_2, and O_2 adsorption isotherms (Table S2-S21 of the Supporting Information) were measured on a commercial volumetric apparatus (Micromeritics ASAP2020). Prior to the measurements, the pure H-ZSM-5 samples (in powder form) and the monolith (in pieces of 0.6 x 0.6 x 0.6 cm) were degassed at 400°C on a vacuum line equipped with a turbomolecular pump and then the samples were transferred in the measurement cell in a glove box. Complete set of CO_2, N_2 and O_2 isotherms as recorded up to 1 bar and different temperatures (25, 60, 90 and 120 °C for CO_2 while only 25, 60 and 90 °C for N_2 and O_2) are reported in Figure S10 of the Supporting Information. The measurements of surface areas and pore volumes were performed dosing N_2 at 77 K till 1 bar. The $T = 77$ K has been reached by means of a liquid nitrogen bath. Temperature control during the measurements in the RT-90°C range was achieved by using an external isothermal liquid bath (Julabo F25-EH), whereas for the 120°C isotherm an external furnace was used. The specific surface area was obtained by using the Langmuir[36, 37] approximation in the standard pressure range ($0.05 < p/p_0 < 0.20$). Although the BET model is not applicable in the standard pressure range for these materials (negative BET constant), the corresponding surface areas have been reported to allow the comparison with previous studies. Pore size distributions (PSD) were evaluated using the Non-Local DFT (Density Functional Theory) method on the basis of the cylindrical pore model proposed by Tarazona[38] on ASAP 2020 V4.00 Software (Micromeritics). The micropore volume (V_{micro}) has been evaluated with the t-plot method adopting the Harkins and Jura equation of thickness in the $0.15 < p/p_0 < 0.50$ range.[36] CO_2 (4.8 N, dry bone purity), O_2 (6.0 N) and N_2 (6.0 N) gases were purchased from Rivoira. In section 5.1 of the Supporting Information we reported the Dual and Single-site Langmuir fit calculations for CO_2, N_2 and O_2 isotherms.

From the fit of CO_2, O_2 and N_2 isotherms reported in Figure 7a, 7b and 7c, the isosteric heat of adsorption q_{st} has been calculated. Details are reported in section S5.2 of the Supporting information.

Microgravimetric measurements. Water isotherms (Table S22-S29 of the Supporting Information) were measured by using an intelligent gravimetric analyzer (IGA-002, supplied by Hiden Analytical Ltd, UK), equipped with a fast heating furnace for the temperature control and an ultrahigh vacuum system (10^{-6} mbar). Before each measurement, the samples was degassed for 6 h at 400°C. Buoyancy corrections were carried out using the weights and densities of all the components of the sample and counterweight sides of the balance and the measured temperature. The water isotherms reported in Figure 8 were interpolated by using a cubic spline function. The used skeletal sample density was measured by liquid pycnometry using water (1.74 ± 0.02 g cm^{-3} for H-ZSM-5 and 1.44 ± 0.02 g cm^{-3} for the monolith).

XRD Powder measurements. X-Ray Powder Diffraction measurements were performed in the 2θ range 2° – 90° (step size of 0.0167°, time per step 200 s) in Debye-Scherrer geometry using a laboratory diffractometer (Panalytical X’Pert Pro Multipurpose Diffractometer) having as source a high powdered ceramic tube PW3373/10 LFF with a Cu anode (Cu $K\alpha$: 0.15418 nm) equipped with a Ni filter to attenuate K_β and focused by a PW3152/63 X-ray mirror. The incident beam was collimated by a soller slit (0.04 rad), an antiscatter slit (1/2 Å) and a divergence slit (1/2 Å); for the diffracted beam an antiscatter slit (AS Slit 5.0 mm, X'Celerator) and a soller slit (0.04 rad) were adopted. Samples were sealed into boron silica glass capillaries of internal diameter 0.8 mm in a protected atmosphere and mounted on a rotating goniometer head.

Differential scanning calorimetry and specific heat capacity. DSC measurements were performed on the pure active phase (H-ZSM-5-800), on the monolith and on Carbon(M) by heating the sample under N_2 flow at 50 ml min^{-1} by means of a DSC Q200 instrument (calibrated at the melting temperature of indium), from 30 to 200 °C (2°C/min ramp). These measurements were important to evaluate the specific heat capacity (c_p) at different temperatures of the tested materials. This physical quantity can be obtained by the scanning method,[39] as described in Section S3 of the Supporting Information (raw data in Table S1 and Figure S6-S8 of the Supporting Information). For this measurement, the tested materials were activated at 400°C and then inserted each time in a standard aluminum sample holder sealed in controlled atmosphere (Glove Box filled with N_2 5.5 purity grade) in order to avoid adsorption of atmospheric contaminants during the sample loading.

Thermogravimetric analysis (TGA) charts have been also conducted on NH_4-ZSM-5 precursor, H-ZSM-500 and the monolith from RT to 900°C in N_2 flow (2°C/min ramp). In the case of the monolith, the flow was switched from N_2 to air for the last hour in order to allow the quantification of the carbonaceous part of the material, as reported in Figure S5, Section S2 of the Supporting Information.

Microcalorimetry. Water adsorption heat was measured at 303 K, with a Tian-Calvet microcalorimeter (Calvet C80, Setaram, France) connected to a grease-free high-vacuum gas-volumetric glass apparatus (residual $p \approx 10^{-4}$ mbar) equipped with a Ceramicell 0-100 mbar gauge (by Varian). The samples were outgassed at 400°C for 6 h. From the heat evolved for each adsorbed amount Δn_a the integral curve $q_{int}(n_a)$ was obtained. The differential heat q_{diff} presented in Figure S16 were obtained by the dose related adsorption heats ($\Delta q_{int}/\Delta n_a$, kJ mol^{-1}) *vs* the middle point of the n_{ads} histogram relative to the individual adsorptive aliquot, prepared as small as possible.

TEM/EDS. Transmission Electron Microscopy analysis was conducted using a JEOL 3010-UHR instrument operating at 300 kV, equipped with a (2k × 2k) pixels Gatan US1000 CCD camera and with an Oxford INCA Energy TEM 200 EDS X-rays analyzer instrument for atomic recognition via energy dispersive spectroscopy (EDS) on the Kα of the elements considered. Quantitative compositional data were obtained using the Oxford INCA Microanalysis Suite software (further details in Figure S4, Section S1.3 of the Supporting Information). For HR-TEM observations, samples where gently milled in an agate mortar. Then, to obtain a good dispersion on the sample holder and avoid any contamination, standard lacey carbon film covered 200 mesh copper grids (Structure Probe, Inc.) were briefly contacted with the powders, resulting in the adhesion of some particles to the sample holders by electrostatic interactions.

Pulse and breakthrough measurements. Diffusion measurements of CO_2, N_2 and O_2 were performed on H-ZSM-5-800 (in form of powder) and on the zeolite–based carbon monolith (in particles having a mesh of 300-500 μm) at 25, 60, 90, 120 °C. While diluted breakthrough experiments were used to determine the diffusion parameters of CO_2, diffusion parameters of O_2 and N_2 were determined by pulse chromatography (Figure S11-S16). The experimental conditions of both experiments are listed in Table S30, Section S6 of the Supporting Information. The flow-rate for diluted CO_2 breakthrough curves (0.5 vol.% CO_2 in He from Yara, Norway) was fixed at 20 and 22.5 ml min^{-1} respectively for the feed gas and for the helium used for desorption. Both H-ZSM-5-800 and the final artifact were pretreated at 200 °C under a flow of helium overnight. The calculations for the dimensionless Henry's law constants of CO_2, O_2 and N_2 are listed in Table S31-S36, Section S6.1 of the Supporting Information. Further details on the diffusion of N_2, O_2 and CO_2 are listed in Table S37, Section S6.2 while mathematical model used to simulate pulses and breakthrough curves is presented in Section S6.3 of the Supporting Information.

IAST selectivity. CO_2/N_2 selectivity factors in the presence of 5 vol.% O_2 were evaluated from the CO_2, N_2 and O_2 single component isotherms fitted through a dual site Langmuir equation (see details in Section S5.1) by the Ideal Adsorbed Solution Theory (IAST)[40] using the pyIAST software.[41] Details on the calculation procedure followed for the IAST calculations are reported in Ref. [41]. The dependence of CO_2/N_2 selectivity factors on CO_2 partial pressure for a ternary $CO_2 : N_2 : O_2$ gas mixture (5 vol.% O_2 gas mixture) at 1 bar and 25, 60 and 90 °C have been obtained for both H-ZSM-5-800 and the monolith by keeping constant the total pressure (1 bar) and the partial pressure of O_2, (0.05 bar) while varying the partial pressure of CO_2 and N_2.

3. Results and Discussions

XRD. Powder XRD patterns of H-ZSM-5-500, H-ZSM-5-800 and the monolith after activation at 400°C are reported in Figure 1. The pattern of NH_4-ZSM-5 – precursor material of the above mentioned H-ZSM-5 zeolite – is also reported for comparison (grey line). In order to obtain the pattern for the monolith, a portion of it was gently grinded in a mortar to preserve the nature of the composite. All the patterns reported in Figure 1 were then normalized to the intensity of the $2\theta = 7.85°$ peak to facilitate their comparison. From the comparison expressed in Figure 1, we can appreciate that the four patterns are very similar. In particular we observe no substantial changes on the samples that incurred on a high temperature treatment (800°C), necessary for the pyrolysis of the resin during the monolith preparation. This result is supported by the well-known resistance of MFI-type zeolites such as ZSM-5 to high temperatures (> 900 °C), because of their low-aluminum content and the absence of Si-O-Si bond angles less than $2\theta = 140°$.[42, 43] The absence of any extra peak and the lack of any peak shift testify also the absence of any phase transition.

As the monolith is constituted by 22% of conductive carbon, the presence of an amorphous phase on the black pattern should be observed as broad halos at about 27°, 42° and 78°.[44] At the best of our inspection – based on the black pattern – none of them is observed. In fact, the detection of an amorphous phase and its eventual quantification cannot be evaluated because of the much higher scattering factor of the zeolite with respect to the amorphous one. This fact is confirmed by Figure S3 of the Supporting information, where a comparison between the XRD patterns of the monolith and the phenolic resin carbonized at 800 °C is shown. Moreover, even if detectable, any amorphous phase deriving from the zeolite or from the carbon phase would overlap with the signals arising from the amorphous glass capillary used in the Debye-Scherrer geometry.

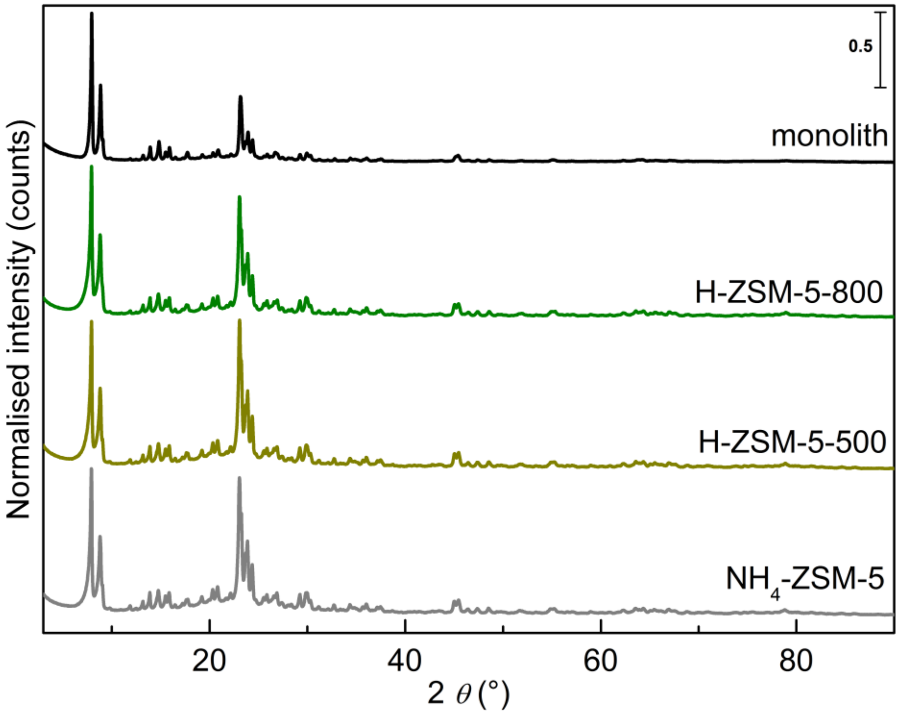

Figure 1. XRPD patterns of NH$_4$-ZSM-5 precursor in air (grey line) and of H-ZSM-5-500 (dark yellow line), H-ZSM-5-800 (green line) and the monolith (black line), activated in vacuum at 400 °C and kept in inert atmosphere. The pattern intensity has been normalized to the 7.85° peak.

Porosity. Nitrogen volumetry at 77 K is used to evaluate the specific surface area, volume and dimension of the pores of a microporous adsorbent. This type of measurement, performed on a series of samples obtained from different treatment conditions, can help to identify an evolution in the textural properties such as the formation of mesoporosity (appearance of hysteresis loop), pore collapse (substantial decrease in microporosity) or change in particle size (decrease of the external surface area). Nitrogen volumetry has been performed on the above-mentioned set of samples and the results are reported in Figure 2 and Table 1. Nitrogen volumetry at 77 K is known to be a more sensitive technique with respect to XRD to evidence small differences in the structure of materials and in particular eventual structure collapse.[45] Moreover, not asking as prerequisite the crystallinity of the sample, it is able to give indications about the way the structure is modified in terms of surface area, pore volume and dimension, even in the case of sample amorphization. Zeolite structure in general collapses because of too harsh conditions causing its dealumination with the consequential creation of a hierarchical (largely amorphous) pore structure and in particular of mesopores. As it can be seen from the comparison of H-ZSM-5-500 (dark yellow line) and H-ZSM-5-800 isotherms (green lines line) in Figure 2, the textural properties of H-ZSM-5 are not strongly affected when treating the zeolite at 800 °C. In fact, both the zeolites present Ib type isotherms, typical of purely microporous materials,[46] confirming that the samples do not encounter extensive damages in the frameworks. The surface areas reported in Table 1 indicate a decrease in the H-ZSM-800 porosity lower than 10%(experimental error) with respect to H-ZSM-5-500. Pore size distribution analysis does not indicate the presence of mesoporosity for H-ZSM-5-500 and H-ZSM-5-800 samples (see Figure S2b in the Supporting Information), as qualitatively suggested by the shape of the isotherms (type Ib).[46] In the case of the monolith, an increase in the microporosity is observed with respect to H-ZSM-5-800; this fact can be easily related to the presence of the conductive carbon (Carbon(M)). It is interesting to notice that the Carbon(M) phase is characterized by a mesoporous/microporous structures on the basis of the nitrogen volumetric measurements (see blue curve in Figure S2 in the Supporting Information) with a contribution of 624 $m^2\ g^{-1}$ of the micropores to the total surface area (1075 $m^2\ g^{-1}$) as obtained by the t-plot analysis. By considering that the carbon content in the monolith amounts to 17 wt.% (see Figure S5a), the Langmuir surface area of the carbonaceous phase can be estimated to be 685 $m^2\ g^{-1}$, that is close to the microporous surface area measured for

Carbon(M) (624 m^2 g^{-1}). Moreover, the N_2 isotherms give some indications about the structure of the carbon: in fact, the hysteresis loop in the monolith isotherm suggests a lamellar structure of the carbon, as expected during the formation of a thin carbon coating on the zeolite surfaces, both on the external and the internal surface.

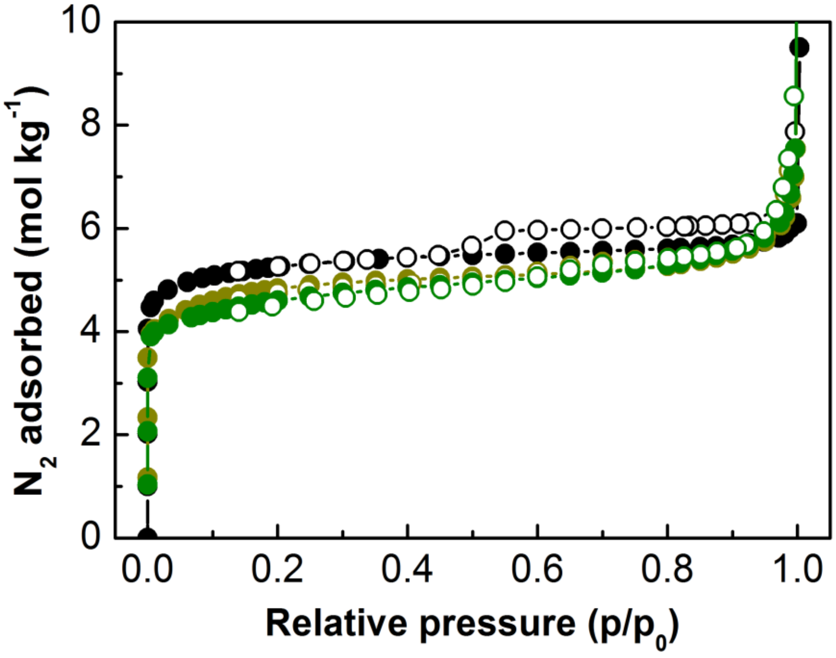

Figure 2. Volumetric N_2 adsorption/desorption isotherms obtained at 77 K for H-ZSM-5-500 (dark yellow curve), H-ZSM-800 (green curve) and the monolith (black curve). Filled and empty scatters refer to adsorption and desorption branches, respectively.

Table 1. BET (S_{BET}, m^2 g^{-1}) and Lanmguir surface areas (S_{Langmuir}, m^2 g^{-1}), total pore volume calculated at p/p_0 = 0.97 (V_{tot}, in cm^3 g^{-1}) and micropore volume (V_{micro}, in cm^3 g^{-1}) of H-ZSM-5-500, H-ZSM-5-800, the monolith and Carbon(M).

	S_{BET}	S_{Langmuir}	V_{tot}	V_{micro}
H-ZSM-5-500	371	492	0.21	0.14
H-ZSM-5-800	350	467	0.21	0.13
monolith	397	528	0.20	0.16
Carbon(M)	801	1075	0.72	0.30

TEM. High resolution transmission electron microscopy (HR-TEM) was used to evaluate the interaction between zeolite particles and the carbonaceous phase, and detect possible modifications occurred to the inorganic phase (zeolite) during the extrusion process. Microscopy allows also visualizing the carbon structure in the monolith. For what concerns H-ZSM-500 and H-ZSM-800, because of the coincidence of the results obtained for the two systems, only the results concerning H-ZSM-5-800 have been reported in the following. Synoptic views of the H-ZSM-5-800 material and of the monolith are displayed in Figure 3, parts (a,) and (b, c), respectively.

At low magnification, the TEM images showed that the projections for both the H-ZSM-5-800 (Figure 3a) and the monolith (Figure 3b and c) particles are similar, exhibiting irregular polygonal shapes, with size ranging from some tens to some hundreds of nm (see section S1.3 of the Supporting Information, Figure S4d and S4e). For the monolith , two images are reported as an example of a number of cases of i) the zeolite almost completely un-blended from the carbon phase (Figure 3b) – even after the gently manual milling – and ii) the zeolite still blended together with the carbon phase (Figure 3c). Concerning the latter, it is worth noticing that zeolite grains (yellow dashed line in Figure 3c) and carbon (orange dashed line in Figure 3c) appeared in quite close contact, with the carbonaceous phase exhibiting the aspect of small flakes which, on the basis of the very pale contrast, might be as thin as a layer few atoms thick. This observation confirms what expected from the shape of the monolith N_2 isotherms (black line, Figure 2) and, on the basis of the XRD results, suggesting a very high dispersion of the carbon. At higher magnification, for both samples the particles exhibited lattice fringes with similar frequency (Figure S4b and S4c), witnessing the crystallinity of the object inspected, and confirming – at the microscopic level – the XRD and N_2 volumetry results presented in the previous section that is the persistence of the crystalline character for the zeolite particles in the monolith.

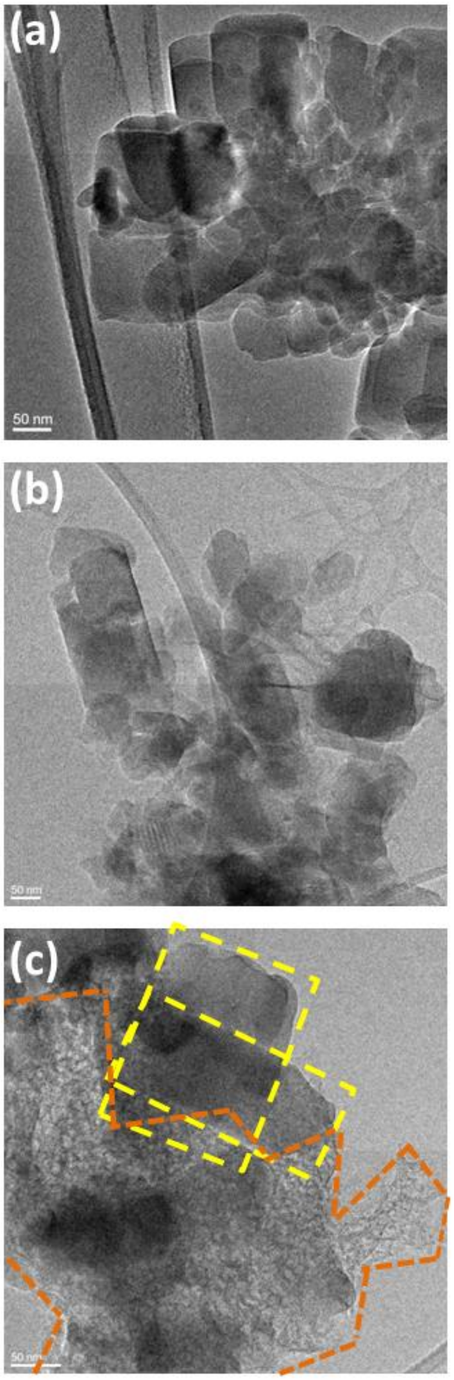

Figure 3. TEM images (original magnification = 30k x) of: (a) H-ZSM-5-800; portions of the monolith showing the zeolite and the carbonaceous part (b) unblended or (c) blended together. In part c, zeolite particles are traced with yellow dashed line while the carbon flakes are traced with orange dashed line.

An EDS analysis of the monolith was carried out, collecting data for both particles and ensemble of particles surrounded by the carbonaceous phase (e.g. Figure 3c), and for particles un-blended from it (e.g. Figure 3b). To obtain statistically reliable data, the number of particles analyzed was increased until the invariance in the distribution of the results was attained (reported in Figure 4 Figure 3). This resulted in the collection of ca. 300 analyses for each group. Sodium was the only extra element found with respect to those constitutive of H-ZSM-5, i.e. Si, Al, and O (besides C). Sodium was present in the phenolic resin and this result indicates that Na^+ ions diffused within the zeolite channels during the monolith synthesis partially exchanging H^+. Its content was evaluated in terms of Na/Al atomic ratio, in order to evaluate the degree of the cation exchange.

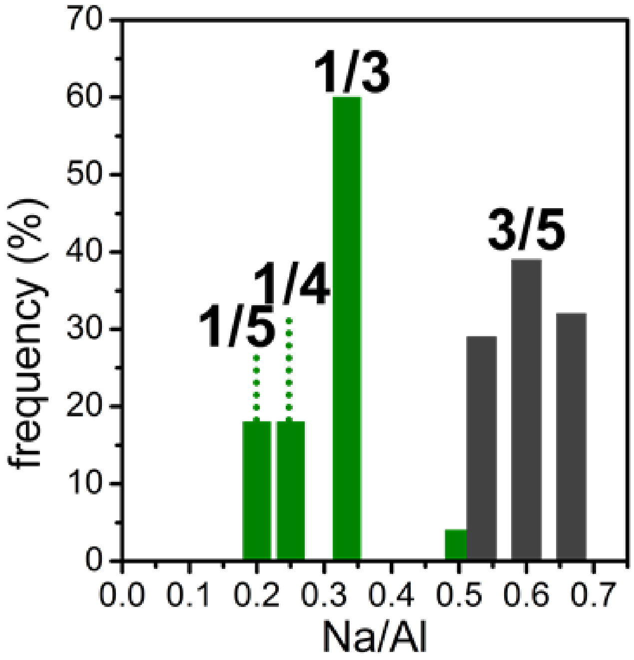

Figure 4. Distribution histograms of the Na/Al atomic ratio in the monolith. Green bars: zeolite particles almost separated from the carbon (e.g. like in Figure 3 part b); grey bars: zeolite particles still embedded in the carbon (e.g. like in Figure 3 part c).

Figure 4shows the distribution histograms of the Na/Al values resulting from the analysis of the zeolite particles surrounded by carbon (grey bars) or (almost) unblended from it (green bars). Focusing on these latter, basically a Na/Al = 1/3 was overwhelmingly found, while the ratio appeared higher when analyzing zeolite particles and carbon still mixed together, witnessing for the presence of Na^+ in the carbonaceous phase.

FTIR. As well known, TEM –as all other types of microscopies – suffers from the limitation of the extremely small amount of sample analyzed (typically, nanograms). Moreover, diffraction and volumetry are not sensitive to small changes in the chemical nature of the sample. Confirmatory evidence of the exchange of original H^+ with Na^+ in zeolitic part of the monolith was sought by IR spectroscopy. In fact, hydroxyl stretching frequency ν(OH) is strongly dependent on the chemical environment of the –OH species and to their acidity. It is then easy to differentiate the protons of i) Brønsted sites (Si-OH-Al, 3615 cm^{-1}) ii) the –OH associated to defect species, i.e. silanols and iii) the –OH associated to extraframework Al^{3+} due to partial dealumination. In our case, the latter might be generated from the high temperature necessary for the monolith preparation (Al-OH, 3670 cm^{-1}). A pictorial representation of H-ZSM-5 structure and of the different, possible hydroxyl species is reported in Figure S1. Among all these species, Brønsted sites are the ones characterized by the higher electrostatic potential and then represent the preferential adsorption sites for incoming molecules as CO_2. A preservation of the structure and of the concentration of the zeolitic counterions is important in order to preserve the affinity of the zeolite toward CO_2 also in the monolith. On the other hand, a cation exchange of the protons with Na^+ suggested by EDS, is expected to cause an increase in the CO_2 affinity with respect to the pure zeolitic form, on the basis of results previously reported for H-ZSM-5 (ΔH_{CO2} = 31.3 kJ mol^{-1}, Si/Al = 11.5)[47] and Na-ZSM-5 (ΔH_{CO2} = 50.0 kJ mol^{-1}).[47] In Figure 5, the spectra obtained for H-ZSM-5-500 (dark yellow line) and H-ZSM-5-800 (green solid line) are reported. In the H-ZSM-5-500 spectrum, the predominant species are the H^+ counterions, doubling in intensity the silanols species signal and with only minor contributions associated to extraframework Al^{3+}. The absence of open extralattice Al (i.e. coordinative unsaturated, highly reactive Al^{3+} sites), was indicated by infrared vibrational characterization at 77 K through N_2 (results not reported in this manuscript), a molecular probe able to detect also very low amount of open Al^{3+} sites.[48] Interestingly, also for H-ZSM-5-800, Al^{3+} was not detected by N_2, confirming what expected on the basis of TEM, XRD and N_2 adsorption results, that indicated only minor effects on the structure deriving from the thermal treatment. Conversely, the comparison of the IR spectra in the ν(OH) region, shows quite a substantial change of the IR profile upon the treatment at 800 °C (see green solid curve in Figure 5). The silanols band becomes slightly sharper, whereas the signal related to Al-OH doubles in intensity with a corresponding decrease of the band related to the strong Brønsted sites. In particular the latter is halved with respect to H-ZSM-5-500, testifying the relevant disappearance of some of the sites that should give preferential interaction towards CO_2. A decrease in the Brønsted sites concentration was suggested also by thermogravimetric analysis on the zeolite where a weight loss was detected over 500 °C (see Figure S5b of the Supporting Information), a temperature where molecular water should not be present anymore. This loss is associated with the partial delaumination of the framework, requiring a decrease of the protons concentration.

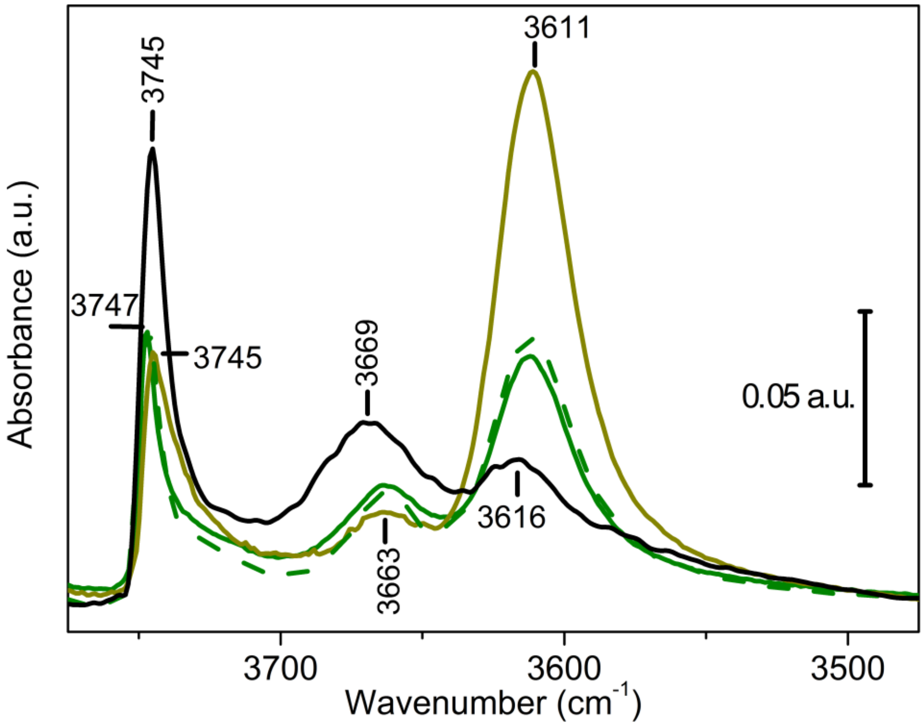

Figure 5. (a) IR spectra of H-ZSM-5-500 (dark yellow line) and H-ZSM-5-800 (green, solid line) in vacuum at RT, after activation at 400°C. It is evident that the intensity of the 3614 cm^{-1} band (related to the strong Brønsted sites) is halved in the H-ZSM-5-800 with respect to the H-ZSM-5-500. The IR spectrum of the monolith recovered from the pyrolysis in O_2 flow of the carbonaceous part (black curve). The spectrum of the H-ZSM-5-800 (green, dotted curve) after a similar treatment is also reported for comparison. All the spectra were normalized with respect to a characteristic pattern in the 2200-1600 cm^{-1} range, due to combination and overtone of vibrational modes of the framework, the intensity of which is then proportional to the amount of sample investigated by the IR beam. The spectra were baseline subtracted by using as baseline a straight line passing for the two extremes of the frequency range reported in the plot.

The monolith was not transparent to the mid-IR radiation because of the presence of conductive carbon. For this reason, before the analysis, the sample was treated in O_2 flow at 500°C in order to pyrolize the carbon: the corresponding spectrum is reported as black curve in Figure 5. For the sake of comparison, the same procedure was repeated on H-ZSM-5-800: the corresponding spectrum (P) is reported as a green dotted line in the same figure. The area of the three main peaks in the OH stretching region for these two samples is reported in Table 2.

Table 2. Position, integrated area and relative changes of relevant ν(OH) bands in the IR spectra of H-ZSM-5-800 (P) and ZSM-5 recovered from the monolith (M). Both the sample were calcinated in O_2 at 500°C before the spectrum recording.

Position (cm^{-1})	**Assignment**	**Integrated area (a.u. cm^{-1})**		**Ratio**	
		H-ZSM-5-800 (P)	**monolith (M)**	**P/M**	**M/P**
3745	Si-OH	1.25	2.21	0.56	1.78
3665	Al-OH	1.11	2.42	0.45	2.20
3614	Si-(OH$^+$)-Al	3.12	2.12	1.48	0.67

It is evident that, although the treatment in O_2 is not able to further affect the H-ZSM-800 spectrum (as demonstrated by the comparison of the solid and the dotted green lines in Figure 5), the band associated to the Brønsted sites is significantly decreased in intensity in the monolith (black line, Figure 5). From the values reported in Table 2, the integrated intensity of this band decreases of about 1/3. The decrease in the proton concentration in the monolith cannot be restricted to dealumination only. TEM/EDS data are thus fully confirmed, suggesting a cation exchange by Na^+ during the monolith synthesis. The IR spectrum of the zeolitic part of the monolith suggests also that the processing for the fabrication of the monolith should have affected in some extent also other parts of the zeolite framework, because an increase of Al-OH and Si-OH defect sites is observed with respect to H-ZSM-5-800. Being these modifications significantly larger with respect to H-ZSM-800(P), it can be inferred that they are related to the chemical environment created by the decomposition of the phenolic resin and not simply to the high temperature conditions required by the pyrolysis.

Specific heat capacity. The specific heat capacity c_p is an important parameter for a material to be used for carbon capture purposes.[3] In fact, when the regeneration of the adsorbent is done by temperature (TSA), the energy required for this step will be directly related to the heat capacity of the material. Water heat capacity (4.18 kJ kg^{-1} $°C^{-1}$) is considered a reference c_p value, being the main component of amine-based scrubbers,[49] nowadays the state-of-the-art technology for post-combustion CO_2-capture.[5] Water is characterized by a very high heat capacity and its use as solvent in these systems is at the basis of the high energy penalty paid in the carbon capture chain. On the other hand, a too low heat capacity can facilitate the creation of hot spots in the material causing its fast degradation.[5] In Figure 6, the specific heat capacity of H-ZSM-5-800 (1, green line) and of the monolith (3, black line) are reported as a function of the temperature and compared to those of other solid sorbents proposed for CO_2-capture technique. The c_p obtained for the pure carbonaceous phase is also reported (2, dark cyan). Details on c_p measurements are reported in Section S3 of the Supporting Information. The zeolite and the composite showed totally different values and dependence of c_p on temperature. The pure zeolitic material (H-ZSM-5-800) has a c_p value of 0.8 kJ kg^{-1} $°C^{-1}$, almost independent on temperature, in the 60-140°C range. The presence of the carbon coating has two main effects: (i) an increase in the c_p values (from 0.8 to 1.1 kJ kg^{-1} $°C^{-1}$, at 60°C) and (ii) a strong dependence of c_p on the temperature. For what concerns point (i), this can be related to a larger degree of freedom for the molecules within the carbonaceous phase with respect to the one of the zeolite phase, as explained by Mu et al.[50] The dependence highlighted in point (ii) can be generally explained through the definition of heat capacity, i.e. a constant that regulates the proportionality between the internal energy of a material and the temperature applied: whenever extra degrees of freedom (such as rotation and vibrations quantized energy modes) are induced in the constituent molecules of a material, the internal energy increases and so does the constant c_p. in order to maintain the proportionality between temperature and internal energy, as explained by the equation S1 in section S3 of the Supporting Information.

This can be the case of carbonaceous phases. In fact, as reported in Figure 6, the c_p trend (slope) of Carbon(M) is reassembled by other another carbonaceous material such as double-walled carbon nanotubes (DWCNTs).

Although the heat capacity contribution of the carbonaceous phase leads to a higher c_p in carbon monolith with respect to the one of zeolite active phase alone (black triangles line vs. green triangles line of Figure 6), the c_p values obtained for the structured adsorbent are still in the range considered interesting for practical applications being only one fourth of that of aqueous solution. To confirm this statement, we reported in Figure 6 the heat capacity of interesting materials for CO_2 capture such as MOF-177,[50] UTSA-16,[12] NaX[51] and Zeolite 4A.[52]In fact, the PSD curve (see Figure) do not evidenced the presence of mesopores also in the monolith.

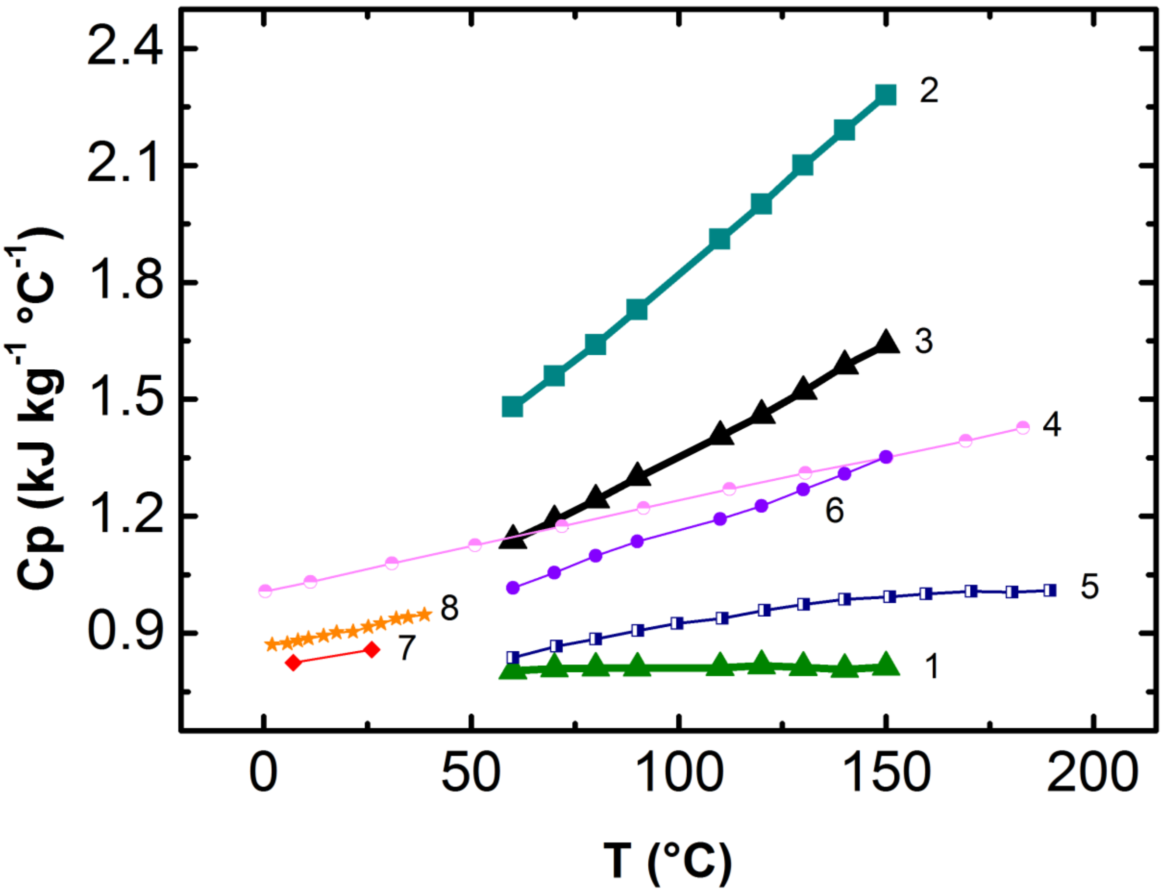

Figure 6. Specific heat capacities of H-ZSM-5-800 (1, green, full triangles, this work), Carbon(M) (2, dark cyan, full squares, this work), carbon monolith (3, black line, full triangles, this work) and of materials proposed for CO_2-capture in the literature: DWCNT (4, light pink line, half circles),[53] MOF-177 (5, blue line, half squares),[50] UTSA-16 (6, violet line, circles),[12] NaX (7, red line, rhombi),[51] Zeolite-4A(8, orange line, stars).[52]

CO_2, O_2, N_2 and H_2O capacity. In order to test the CO_2 affinity of the monolith with respect to its parent material (H-ZSM-5), a series of CO_2, N_2, O_2 volumetric adsorption measurements has been recorded at pressure range 0-1 bar and within the temperature range of interest (25-120°C). These isotherms have been reported in Figure 7a. The results obtained on H-ZSM-5-500 and H-ZSM-5-800 were fully comparable for all the adsorbates considered at RT (see Figure S9 in the Supporting Information). For this reason, the full volumetric characterization was performed only for H-ZSM-5-800.

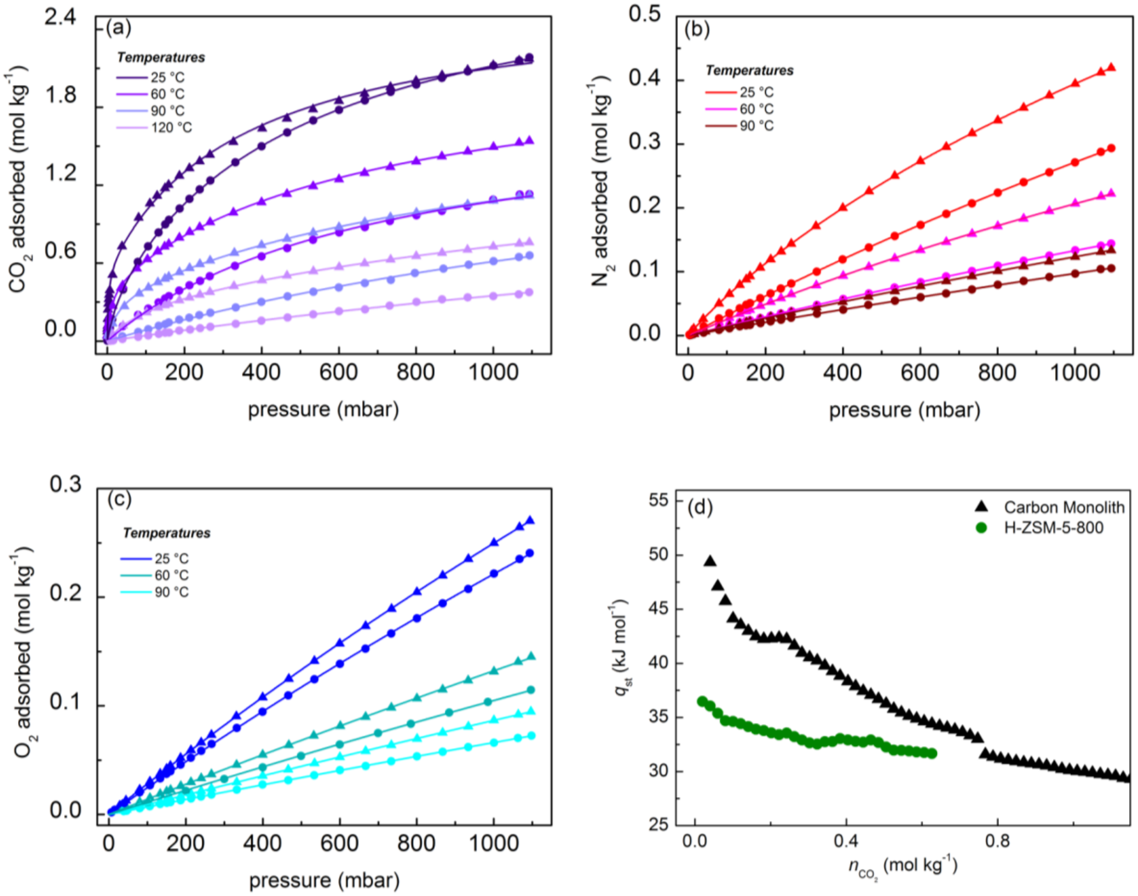

Figure 7. (a) CO$_2$, (b) N$_2$ and (c) O$_2$ adsorption isotherms on H-ZSM-5-800 (●) and the monolith (▲) at 25, 60 and 90 and 120 °C (at 120 °C only for CO$_2$. CO$_2$ color code: from dark violet (25 °C) to light violet (120 °C). N$_2$ color code: red (25 °C), magenta (60 °C) and dark red (90 °C). O$_2$ color code: blue (25 °C), dark cyan (60 °C) and cyan (90 °C). Desorption branches are reported in Figure S10 of the Supporting Information. Continuous lines has been obtained from the Dual and Single-site Langmuir fits (details are listed in section S5.1 of the Supporting Information) (d) CO$_2$ isosteric heat of adsorption calculated by fitting the isotherms reported in part (a) for H-ZSM-5-800 (green scatter) and the monolith (black scatter). The q_{st} has been calculated up to the coverage that allowed the fit of at least 3 points (details of q_{st} calculation are listed in section S5.2 of the Supporting Information).

For what concerns CO$_2$, a capacity of 2.2 mol kg^{-1} was obtained at 25°C and 1.1 bar for both the monolith (triangles in Figure 7a) and the H-ZSM-5-800 (circles); nevertheless a different shape of the isotherms can be noted, suggesting a higher affinity toward CO_2 of the monolith, being the CO_2 capacities higher for the latter at $p \leq 0.2$ bar, which the typical partial pressure range for CO_2 in a post-combustion flue gas. This is particularly interesting because it shows how the adsorption properties of a material would be underestimated if evaluated on the basis of the pure active phase alone; it is then important to study the adsorption characteristic of an adsorbent which was previously molded in a shape as close as possible to the one that will be actually employed. The gap in the adsorption properties between the pure active phase alone and the final artifact (i.e. zeolite-based carbon monolith), is even more pronounced when we consider the curves obtained at higher temperatures (as illustrated the curves of lighter violet in Figure 7a). In fact, for higher temperatures, a larger CO_2 uptake is observed along the whole isotherm for the monolith with respect to H-ZSM-5-800. The explanation of this behavior can be associated to the fact that, as described in the previous section, upon the preparation of the honeycomb, some Na^+ replaced protons in the pristine H-ZSM-5 giving rise to the formation of a H-Na-ZSM-5, where Na can exert a higher electric field towards CO_2 than protons (4.8 vs. 3 V nm^{-1}).[54] In addition to the presence of Na^+ (replacing some H^+), also the presence of a higher amount of local defects (increase of silanols) and partial extra framework OH groups, could give some beneficial effect to the adsorption properties of the final material.

Figure 7b and c show N_2 and O_2 adsorption isotherms at 0-1 bar and different temperatures for both H-ZSM-5-800 (circles) and the monolith (triangles). Despite the fact that the adsorbed quantities of these gases are much lower than those registered for CO_2, the higher N_2 (or O_2) uptake of the monolith with respect to H-ZSM-5-800 is still remarkable. As this affects the selectivity factors in the two samples was evaluated with the Ideal Adsorbed Solution Theory (IAST) analysis (see below).

Water is one of the components of the flue gases that largely affects the CO_2 adsorption properties of a material. In fact, water is preferentially adsorbed by materials, lowering the CO_2 storage properties. Increasing the material hydrophobicity is a strategy to improve its CO_2-captureperformances in presence of a real flue gas flow. Gravimetric adsorption isotherms of water are reported in Figure 8 for H-ZSM-5-800 (part a) and the monolith (part b) from 25 to 120 °C and partial pressure up to 22 mbar at 25°C and 45 mbar for $T > 25$°C.

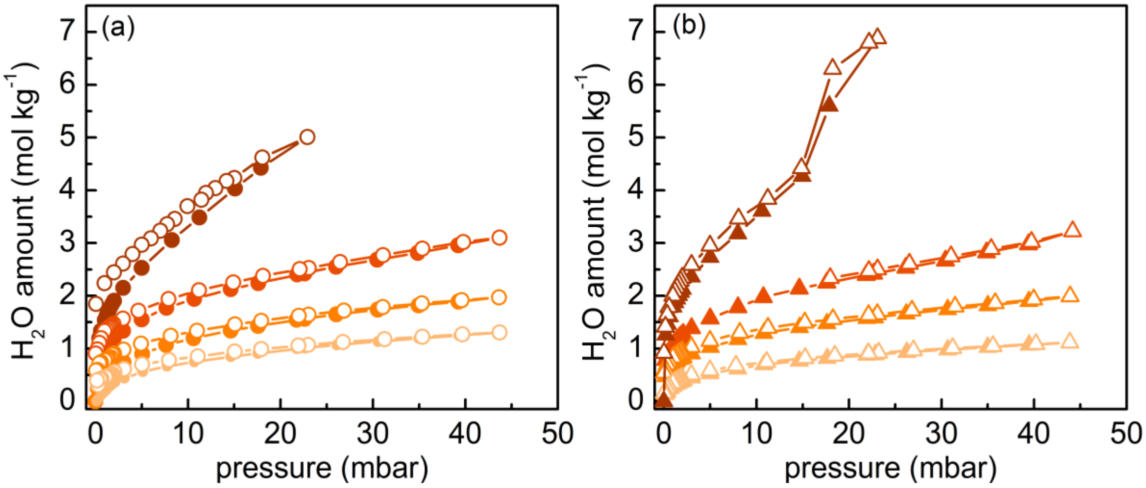

Figure 8. H_2O adsorption (full dots) and desorption (empty dots) isotherms of H-ZSM-5-800 (a) and the monolith (b) at 25, 60, 90 and 120 °C. Color code: from dark orange (25 °C) to light orange (120 °C).

From the comparison between the two samples it is evident that the presence of the carbon has two main effects on the water adsorption isotherm: (i) change in the adsorption capacity; (ii) change in the shape of the isotherm. These two effects are different at the different temperatures because of the different p/p_0 ranges considered (p_0 = 0.7, 0.2, 0.08 and < 0.04 at 25, 60, 90 and 120°C respectively). For what concerns the 90 and 120°C isotherms, a lower capacity is verified for the monolith with respect to the zeolite. On the contrary, in the 25 and 60°C isotherms, the maximal water capacity is increased in the monolith with respect to the zeolite. Moreover, also the position and shape of the hysteresis loop is significantly different: a "S" shaped upper curve related to water capillary condensation within the carbon framework pores is visible for the monolith recalling the typical isotherm shape of activated carbons. The relative pressure α at which half of the total water capacity is reached in a material is a good indicator of the hydrophobicity of such a material;[55] the higher is this value the higher will be the hydrophobic character. The total water capacity was estimated from the material micropore volume to 7.8 and 16.8 mol kg^{-1}, for H-ZSM-5-800 and the monolith, respectively. α would correspond to 12 mbar for H-ZSM-5-800, whereas it would be definitely larger for the monolith (outside the pressure range considered), characterized by a larger hydrophobicity. The hysteresis loop closes at about 15 mbar for the monolith, whereas it closes at pressure lower than 1 mbar in the case of the zeolite suggesting as the presence of the carbon would facilitate the complete reactivation of the material upon degassing. Another important point is related to the dependence upon temperature of the isotherms in the two materials: in fact, as mentioned above, since the water capacity is lower for the monolith than for H-ZSM-5-800 at 90 and 120°C, a larger working capacity is expected for the monolith by reactivation upon thermal heating. This datum is quite meaningful in terms of post-combustion CO_2-capture where H_2O is present in 5-7 vol.%.[33] The material affinity for water was also evaluated by means of microcalorimetric measurements (see Figure S17). Accordingly, the heat of adsorption in the zeolite (121 kJ mol^{-1}) is 20% higher than in the monolith (96 kJ mol^{-1}). These values are close to those previously reported for ZSM-5 zeolites.[56] Literature values always indicate a lower water affinity for Na- than for H-ZSM-5,[56] suggesting that not only the presence of the carbonaceous phase, but also the H^+ to Na^+ exchange contributes to the increased hydrophobicity of the monolith.

Diffusion measurements. Breakthrough and pulse chromatography measurements.

In gas adsorption, the Henry's law constant (K_H) is defined as another way to establish the affinity of an adsorbate towards an adsorbent surface. In this study, K_H has been evaluated for CO_2, N_2 and O_2 by means of diluted breakthrough (Figure 9a) and pulse chromatography experiments (Figure 9b,c) for both H-ZSM-5-800 and the monolith. These measurements were performed in the 25-120 °C temperature range, analogously to the static volumetric measurements (see Section 6 of the Supporting Information).

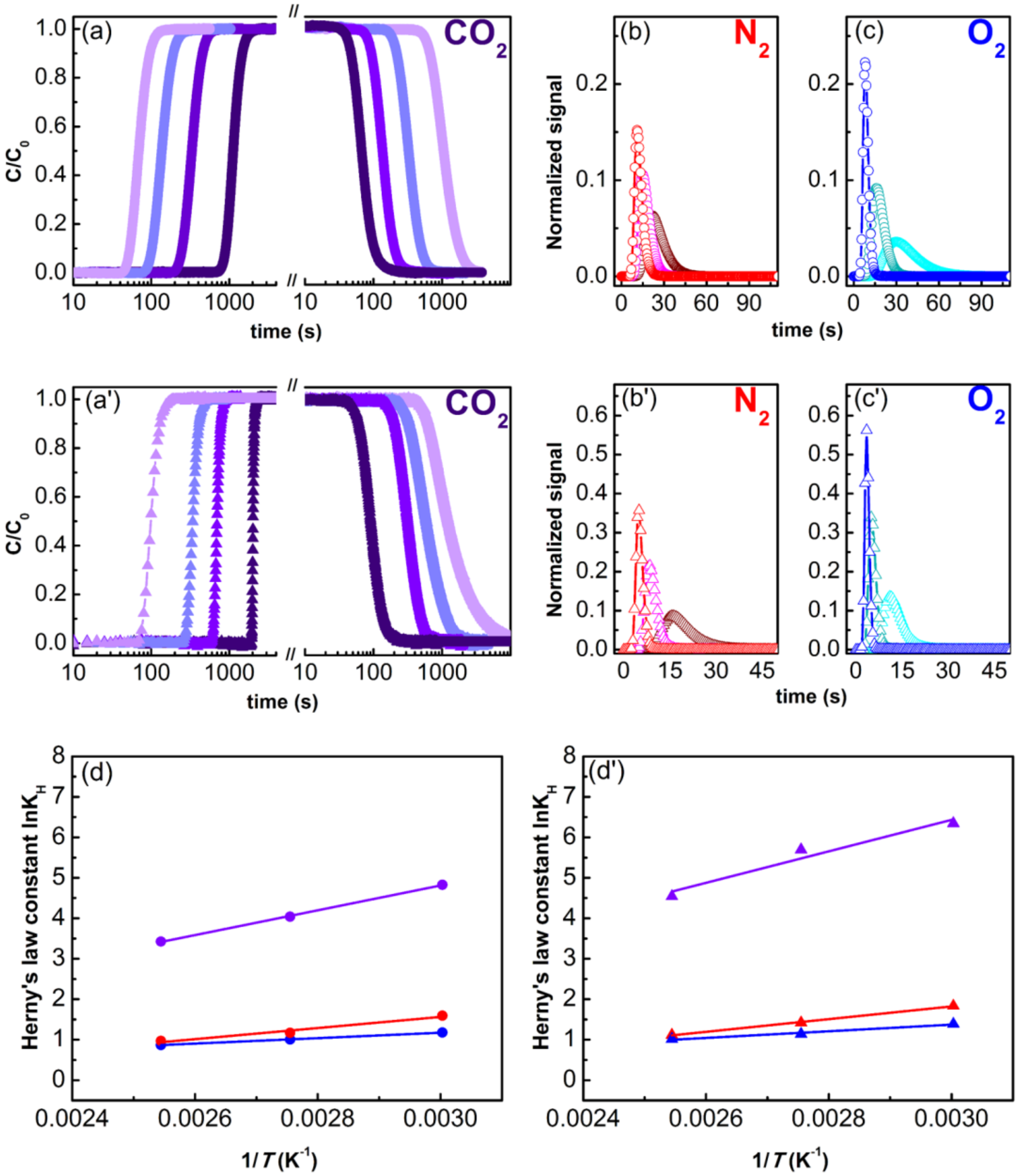

Figure 9. Experimental CO_2 breakthrough adsorption/desorption curves (0.5 vol.% CO_2 in He) on (a, ●) H-ZSM-5-800 and (a', ▲) the monolith at 25, 60, 90 and 120 °C. Color code: from dark violet (25 °C) to light violet (120 °C). X-axis is reported in logarithmic scale. Experimental (symbols) and model (continuous line) data for N_2 and O_2 pulse chromatography on (a' and a'') H-ZSM-5 and on (b' and b'') the monolith at 60 °C. The pulse chromatography curves show the signal dependence of the flow: 10 (blue for O_2 and red for N_2), 20 (cyan for O_2 and magenta for N_2) and 30 ml min^{-1} (dark cyan for O_2 and wine for N_2). The natural logarithm of the Henry's law constant K_H is plotted against 1/T for H-ZSM-5 (d, ●) and for the monolith (d', ▲) in the T range 60-120 °C. K_H has been evaluated for CO_2 (violet), N_2 (red) and O_2 (blue). Symbols refer to experimental points while continuous line represents the linear fit.

Figure 9d and Figure 9d' represent the variation of $ln\mathrm{K_H}$ with respect to $1/T$, for H-ZSM-5-800 and the monolith respectively. As expected, the $\mathrm{K_H}$ values decrease with the increasing of the temperature. Furthermore, focusing on the Tables S31 to S36 in the Supporting Information, we can notice how $\mathrm{K_H}$ for CO_2 are at least one order of magnitude higher than those of N_2 and O_2 testifying the higher affinity of both H-ZSM-5 and the monolith to CO_2 with respect to N_2 and O_2. The affinity of CO_2 towards the adsorbent is evidently higher in the case of the monolith than for H-ZSM-5 pure active phase: this result is in line with the presence of Na^+ cations, as previously discussed in the TEM/EDS and FTIR section.

Breakthrough and pulse chromatography experiments were also useful to evaluate the diffusivity of CO_2, N_2 and O_2 within H-ZSM-5-800 pure active phase and the monolith. The diffusivity parameters obtained are listed in Table S37. It is interesting to notice that the diffusivity parameters of CO_2, N_2 and O_2 are very high for both the H-ZSM-5-800 and the carbon monolith. The fast diffusion of CO_2 is an important feature in view of an employment of these materials for real applications. A promising material for CO_2-capture in which similar values of diffusivity were obtained is UTSA-16 (0.015 s^{-1} at 60 °C).[57]

4. Discussions

Isosteric heat of adsorption. To evaluate the relative affinity of CO_2, N_2 and O_2 for the monolith and H-ZSM-5-800, the isosteric heat of adsorption has been calculated (details reported in section 5.1 if the Supporting Information). The values obtained at the lowest coverage, which represent the interaction of the adsorbates with the strongest interaction sites, are reported in Table 3. These values have been obtained from the adsorption isotherms reported in Figure 7a, 6b and 6c, respectively.

For what concerns CO_2, the isosteric heat calculated for H-ZSM-5-800 is close to the one reported previously for H-ZSM-5 by Dunne et al. (ΔH_{CO2} = 38.0 kJ mol^{-1}, Si/Al = 30).[54] For the monolith, an isosteric heat significantly higher than that of H-ZSM-5-800 is obtained. Interestingly, this value is close to the adsorption enthalpy reported in the literature for Na-ZSM-5 (ΔH_{CO2} = 50.0 kJ mol^{-1}),[47,54, 58] confirming the ion exchange hypothesized on the basis of the EDS and IR spectroscopies results. In Figure 7d, the dependence of the CO_2 q_{st} on the coverage is also reported. Supposing that the initial Si/Al = 30 ratio is maintained in the zeolite structure, the full coverage of the counterions with the formation of 1:1 adduct is expected at 1.39 mol kg^{-1} in H-ZSM-5-800 and 1.08 mol kg^{-1} in the monolith. The curves in Figure 7d suggest that the H-ZSM-5-800 sample is characterized by a large homogeneity of the adsorption sites, whereas the monolith surface is largely heterogeneous. The presence of sodium as counter-cation, accompanied by the increase of silanols and partial extra-framework aluminum observed in the monolith, leads to a higher chemical interaction towards CO_2 than the one registered for H-ZSM-5-800 where the role of counter cation is played only by protons, and a lower amount of silanols and partial extra-framework aluminum sites are present.

In particular, an estimation of the degree of the H^+ to Na^+ exchange can be inferred from this graph in about 0.25 mol kg^{-1}, i.e. one fourth of the total counterions, This result is in agreement with what found by means of IR and EDS spectroscopies, allowing then to describe the zeolitic phase in the monolith as a highly defective H-Na-ZSM-5.

The N_2 heat of adsorption on H-ZSM-5-800 is instead slightly lower than the energetic value reported in the literature by means of variable temperature IR methods (19.7 ± 0.5 kJ mol^{-1} on H-ZSM-5 and or 20 ± 1 kJ mol^{-1} on H-FER)):[59, 60] this fact can be related to the different way the two methods allow the adsorption affinity determination. Methods based on IR are site specific:

in particular, in this case only the energetics of the most energetic surface sites (protons) was considered. For what concerns the isosteric heat, it can be seen as an average on all the sites contributing to the interaction at a certain pressure.

For what concerns the O_2 isosteric heats obtained for both the zeolite (14 kJ mol^{-1}) and the monolith (15 kJ mol^{-1}), the values are close to the adsorption heat reported for other zeolitic systems as silicalite (16.3 kJ mol^{-1}) and NaX (15.0 kJ mol^{-1}).[54]

From the comparison of the data reported in Table 3 it is evident that O_2 and N_2 have a significantly lower affinity towards both the zeolite and the monolith with respect to CO_2. Analogously to what previously discussed for CO_2, we denoted an increase in the affinity of both N_2 and O_2 towards the monolith, because of the presence of Na^+ ions. The N_2 q_{st} calculated in our study is very close to the average value obtained by Newsome and Coppens on a Na-ZSM-5 zeolite with slightly lower Si/Al ratio (23-25 kJ mol^{-1} with Si/Al ratio = 45)[58] or by Dunne et al. (24.1 kJ mol^{-1} with Na-ZSM-5 with Si/Al ratio = 30)[54] indicating how the difference in Si/Al ratio does not impact too much on the N_2 energetic of adsorption. It is interesting to notice that whereas in the zeolite the q_{st} of N_2 and O_2 are quite identical, in the monolith the q_{st} of N_2 is appreciably larger than for O_2 (24 vs. 15 kJ mol^{-1}). This is also evident from the isotherms reported in Figure 7b and c, showing that whereas in the zeolite the N_2 and O_2 capacities are very similar at all the pressures, in the monolith the N_2 adsorbed amount are always larger than the O_2 one in the same pressure and temperature conditions.

Table 3. Energetic of adsorption at the lower coverage for different adsorbates towards H-ZSM-5-800 and the monolith.

Material	**q_{st} CO_2 (kJ mol^{-1})**	**q_{st} O_2 (kJ mol^{-1})**	**q_{st} N_2 (kJ mol^{-1})**	**q_{st} H_2O (kJ mol^{-1})**
H-ZSM-5-800	37±4[a]	14±1[a]	15±1[a]	120±10[b]
Monolith	49±5[a]	16±2[a]	24±2[a]	96±9[b]

[a]Isosteric heat, [b]microcalorimetry.

IAST Selectivity. The employment of any adsorbent material within post-combustion CO_2-capture requires a high selectivity for CO_2 towards the other components of a post-combustion gas stream; above all, the selectivity over N_2 is crucial, being this gas the most abundant in a post-combustion mixture (75 vol.%). The selectivity of H-ZSM-5-800 and of the monolith for CO_2/N_2 separation – in the presence of 5 vol.% O_2– were calculated by the use of IAST.[40, 41] The power of IAST is to simulate multi-component isotherms at the desired composition (e.g. 15 vol.% CO_2, 80 vol.% N_2, 5 vol.% O_2) using, as initial guess, the single component isotherms obtained experimentally (in our case reported in Figure 7a, 7b and 7c).

The IAST CO_2/N_2 selectivity in the presence of 5 vol.% O_2 has been calculated by means of pyIAST software[41] for both H-ZSM-5-800 and the monolith, keeping the total pressure of 1 bar constant and varying the CO_2 and N_2 partial pressures. Figure 10 reports the selectivity factors for increasing CO_2 partial pressures.

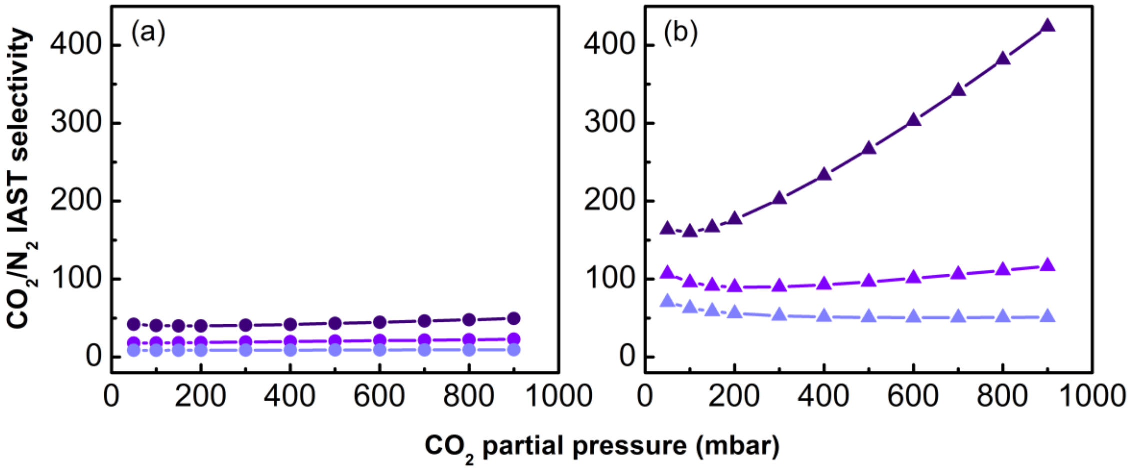

Figure 10 IAST CO_2/N_2 selectivity factors for a ternary $CO_2 : N_2 : O_2$ gas mixture (5 vol.% O_2 gas mixture) at 1 bar and 25 (dark violet line), 60 (violet line) and 90 °C (light violet line) calculated from single component isotherms reported in Figure 7a, 6b and 6c, for increasing CO_2 partial pressure. In the (a) part the data calculated on the H-ZSM-5-800 are represented while on the (b) part the one on the monolith are reported.

Figure 10 is showing how the IAST CO_2/N_2 selectivity of the monolith is, at any temperature, about three times than in the zeolite. These results suggest that also on this point of view, the inclusion of the active phase in the final monolith has brought to a significant modification of its CO_2-capture performances that is an improvement.

5. Conclusions

Several materials have been proposed for carbon capture but only few of them are conductive and then suitable for their implementation in plants using ESA (electric swing adsorption). Moreover, their incorporation as active phase in conductive carbons-based composites requires them to bear the high temperatures involved during the manufacturing process (important for the formation of the carbon phase); these temperatures are often out of the range of the thermal stability of these adsorbents. In this work, the incorporation of H-ZSM-5 in a conductive carbon/zeolite composite has been studied. The composite (78 wt.% of zeolite and 22 wt.% of conductive carbon) has been obtained in a honeycomb monolith form, suitable for its final use in a ESA CO_2-capture process. Besides a lower electric resistivity (5.8 Ω m versus 2500 Ω m),[61] the monolith showed (i) improved CO_2 capacity, (ii) higher water working capacity; (iii) higher CO_2 interaction energy, (iv) higher specific heat capacity. In particular, XRD, TEM and N_2 volumetry indicated that the zeolite structure was almost unaffected by the monolith preparation process. TEM/EDS and IR spectroscopy suggested the possibility that one third of the protons was exchanged by Na^+ ions during the pyrolysis step. A homogeneous grafting of the carbon phase over the active phase was revealed by TEM images acquired at different magnifications.

CO_2 adsorption capacity of the honeycomb reference material was tested by means of volumetric measurements till 1 bar and different temperatures (25, 60, 90 and 120°C). At room temperature and 1 bar, the composite material is up-taking the same amount of CO_2 as the one registered for the pure zeolite; conversely, a higher CO_2 uptake at 0.15 bar (+25 % of CO_2 adsorbed) is observed for the monolith. Volumetric curves associated to the measurements performed at higher temperatures always show higher profiles in case of honeycomb composite materials (1.5 vs 1.1 mol g^{-1} at 60 °C for the honeycomb monolith and for the H-ZSM-5-800 zeolite, respectively). This can be related, besides to the higher defectivity of the monolith (and then higher concentration of Si-OH and Al-OH species), to the higher affinity of CO_2 towards sodium as counter-cation with respect of protons.

Although the monolith shows also a higher uptake of N_2 and O_2 with respect to H-ZSM-5-800, the monolith IAST CO_2/N_2 selectivity (in the presence of 5 vol.% of O_2) is higher than for the zeolite, at any temperature tested.

For what concerns water adsorption, a larger working capacity was predicted for the monolith than for the zeolite, due to the lower adsorption heat: this would suggest an easier removal of water contaminants (among the most energetics adsorbates in the flue gas) from the monolith, and then a less energy-demanding regeneration of the adsorbent in operative conditions.

As a final remark, this work underlined the properties gap between a pure active phase (the zeolite) and its related final artifact. This pointed out the importance of studying the adsorption properties of a sample designed to have shapes and physical-chemical characteristics as close as possible to the material that will be actually employed. This point is particularly important for engineer plant simulations, because the employment of parameters obtained on the active phase could bring to significant error in the process design.

ASSOCIATED CONTENT

Supporting Information. Pictorial representation of H-ZSM-5 structure, Particle distribution size from HRTEM, Thermogravimetric analysis of NH_4-ZSM-5 and the monolith, Specific heat capacity calculation, Adsorption isotherms at 25 °C of CO_2, N_2 and O_2, Calculation of the adsorption enthalpy of O_2 and N_2 on H-ZSM-5-800 by VTIR method, Data tables for CO_2, H_2O, N_2 and O_2 adsorption isotherms, Microcalorimetry of H_2O. This material is available free of charge via the Internet at http://pubs.acs.org.

AUTHOR INFORMATION

Corresponding Author

*Department of Chemistry, NIS Center and INSTM, University of Torino, via Quarello 15, I-10135 Torino, Italy, Tel.: +390116708375, Fax: +390116707855; E-mail: jg.vitillo@gmail.com.

Author Contributions

The manuscript was written through contributions of all authors. All authors have given approval to the final version of the manuscript.

Funding Sources

The research leading to these results has received funding from the European Union Seventh Framework Programme (FP72007–2013) under Grant Agreement 608534 (MATESA project).

ACKNOWLEDGMENT

Maria Botavina and Lorenzo Mino are acknowledged for the help in infrared spectroscopic measurements. Jean-Jacques Theron, Corning, France is acknowledged for proving the materials used in the study. The research leading to these results has received funding from the European Union Seventh Framework Programme (FP72007–2013) under Grant Agreement 608534 (MATESA project).

ABBREVIATIONS

XRD, X-Ray Powder Diffraction; FTIR, Fourier-transformed infrared; MIR, medium infrared; DSC, Differential Scan Calorimetry, CCS, Carbon Capture and Sequestration.

REFERENCES

1. Thiruvenkatachari, R.; Su, S.; An, H.; Yu, X. X., Post combustion CO_2 capture by carbon fibre monolithic adsorbents. *Prog. Energy Combust. Sci.* **2009,** 35, 438-455.
2. Vitillo, J. G., Magnesium-based systems for carbon dioxide capture, storage and recycling: from leaves to synthetic nanostructured materials. *RSC Adv.* **2015,** 5, 36192-36239.
3. Sumida, K.; Rogow, D. L.; Mason, J. A.; McDonald, T. M.; Bloch, E. D.; Herm, Z. R.; Bae, T. H.; Long, J. R., Carbon Dioxide Capture in Metal-Organic Frameworks. *Chem. Rev.* **2012,** 112, 724-781.

4. Samanta, A.; Zhao, A.; Shimizu, G. K. H.; Sarkar, P.; Gupta, R., Post-Combustion CO_2 Capture Using Solid Sorbents: A Review. *Ind. Eng. Chem. Res.* **2012,** 51, 1438-1463.

5. Rochelle, G. T., Amine Scrubbing for CO_2 Capture. *Science* **2009,** 325, 1652-1654.

6. DOE/NETL, Quality guidelines for energy system studies: CO_2 impurity design parameters, Technical report. **2013**.

7. Nikolaidis, G. N.; Kikkinides, E. S.; Georgiadis, M. C., Model-Based Approach for the Evaluation of Materials and Processes for Post-Combustion Carbon Dioxide Capture from Flue Gas by PSA/VSA Processes. *Ind. Eng. Chem. Res.* **2016,** 55, 635-646.

8. Garcia, E. J.; Perez-Pellitero, J.; Jallut, C.; Pirngruber, G. D., Modeling Adsorption Properties on the Basis of Microscopic, Molecular, and Structural Descriptors for Nonpolar Adsorbents. *Langmuir* **2013,** 29, 9398-9409.

9. Huck, J. M.; Lin, L. C.; Berger, A. H.; Shahrak, M. N.; Martin, R. L.; Bhown, A. S.; Haranczyk, M.; Reuter, K.; Smit, B., Evaluating different classes of porous materials for carbon capture. *Energy Environ. Sci.* **2014,** 7, 4132-4146.

10. Fang, H. J.; Kulkarni, A.; Kamakoti, P.; Awati, R.; Ravikovitch, P. I.; Sholl, D. S., Identification of High-CO2-Capacity Cationic Zeolites by Accurate Computational Screening. *Chem. Mat.* **2016,** 28, 3887-3896.

11. Mason, J. A.; Sumida, K.; Herm, Z. R.; Krishna, R.; Long, J. R., Evaluating metal-organic frameworks for post-combustion carbon dioxide capture via temperature swing adsorption. *Energy Environ. Sci.* **2011,** 4, 3030-3040.

12. Masala, A.; Vitillo, J. G.; Bonino, F.; Manzoli, M.; Grande, C. A.; Bordiga, S., New insights into UTSA-16. *Phys. Chem. Chem. Phys.* **2016,** 18, 220-227.

13. Das, A.; D'Alessandro, D. M., Tuning the Functional Sites in Metal-Organic Frameworks to Modulate CO_2 Heats of Adsorption. *Crystengcomm* **2015,** 17, 706-718.

14. Masala, A.; Grifasi, F.; Atzori, C.; Vitillo, J. G.; Mino, L.; Bonino, F.; Chierotti, M. R.; Bordiga, S., CO_2 Adsorption Sites in UTSA-16: Multitechnique Approach. *J. Phys. Chem. C* **2016,** 120, 12068-12074.

15. Bolis, V., Fundamentals in Adsorption at the Solid-Gas Interface. Concepts and Thermodynamics. In *Calorimetry and Thermal Methods in Catalysis*, Auroux, A., Ed. Springer Berlin Heidelberg: Berlin, 2013; Vol. 154, pp 3-50.

16. Khurana, M.; Farooq, S., Simulation and optimization of a 6-step dual-reflux VSA cycle for post-combustion CO_2 capture. *Chem. Eng. Sci.* **2016,** 152, 507-515.

17. Akhtar, F.; Keshavarzi, N.; Shakarova, D.; Cheung, O.; Hedin, N.; Bergstrom, L., Aluminophosphate monoliths with high CO_2-over-N_2 selectivity and CO_2 capture capacity. *RSC Adv.* **2014,** 4, 55877-55883.

18. Rezaei, F.; Webley, P., Structured adsorbents in gas separation processes. *Sep. Purif. Technol.* **2010,** 70, 243-256.

19. Rezaei, F.; Webley, P. A., Optimal design of engineered gas adsorbents: Pore-scale level. *Chem. Eng. Sci.* **2012,** 69, 270-278.

20. Menard, D.; Py, X.; Mazet, N., Activated carbon monolith of high thermal conductivity for adsorption processes improvement Part A: Adsorption step. *Chem. Eng. Process.* **2005,** 44, 1029-1038.

21. Grande, C. A.; Rodrigues, A. E., Electric Swing Adsorption for CO_2 removal from flue gases. *Int. J. Greenh. Gas Control* **2008,** 2, 194-202.

22. Ruthven, D. M., Past progress and future challenges in adsorption research. *Ind. Eng. Chem. Res.* **2000,** 39, 2127-2131.

23. Brandani, F.; Rouse, A.; Brandani, S.; Ruthven, D. M., Adsorption kinetics and dynamic behavior of a carbon monolith. *Adsorpt.-J. Int. Adsorpt. Soc.* **2004,** 10, 99-109.

24. Gorbach, A. B.; Stegmaier, M.; Eigenberger, G.; Hammer, J.; Fritz, H. G., Compact pressure swing adsorption processes-impact and potential of new-type adsorbent-polymer monoliths. *Adsorpt.-J. Int. Adsorpt. Soc.* **2005,** 11, 515-520.

25. Grande, C. A.; Cavenati, S.; Barcia, P.; Hammer, J.; Fritz, H. G.; Rodrigues, A. E., Adsorption of propane and propylene in zeolite 4A honeycomb monolith. *Chem. Eng. Sci.* **2006,** 61, 3053-3067.

26. Li, Y. Y.; Perera, S. P.; Crittenden, B. D., Zeolite monoliths for air separation part 2: Oxygen enrichment, pressure drop and pressurization. *Chem. Eng. Res. Des.* **1998,** 76, 931-941.

27. Gadkaree, K. P., Carbon honeycomb structures for adsorption applications. *Carbon* **1998,** 36, 981-989.

28. Kreutzer, M. T.; Kapteijn, F.; Moulijn, J. A., Shouldn't catalysts shape up? Structured reactors in general and gas-liquid monolith reactors in particular. *Catal. Today* **2006,** 111, 111-118.

29. Klett, J. W.; Burchell, T. D., Carbon fibre carbon composites for catalyst supports. . In *Proceedings of the 22nd biennial conference on carbon*, Pergamon Press, University of California: San Diego, CA, 1995.

30. Thakkar, H.; Eastman, S.; Hajari, A.; Rownaghi, A. A.; Knox, J. C.; Rezaei, F., 3D-Printed Zeolite Monoliths for CO2 Removal from Enclosed Environments. *ACS Appl. Mater. Interfaces* **2016,** 8, 27753-27761.

31. Couck, S.; Lefevere, J.; Mullens, S.; Protasova, L.; Meynen, V.; Desmet, G.; Baron, G. V.; Denayer, J. F. M., CO2, CH4 and N-2 separation with a 3DFD-printed ZSM-5 monolith. *Chem. Eng. J.* **2017,** 308, 719-726.

32. Bagley, R., Method of forming an extrusion die. In Patent US3803951: 1974.

33. Lachman, I. M.; Lewis, R. M., Anisotropic cordierite monolith. In US3885977 A: 1975.

34. Andrzej Cybulski, J. A. M., *Structured Catalysts and Reactors*. CRC Press 2005; p 856.

35. Farrauto, R. J.; Heck, R. M., Catalytic converters: state of the art and perspectives. *Catal. Today* **1999,** 51, 351-360.

36. Gregg, S. J.; Sing, K. S. W., *Adsorption surface area and porosity*. 2nd ed.; Academic Press Inc.: London, 1982.

37. Langmuir, I., The adsorption of gases on plane surfaces of glass, mica and platinum. *J. Amer. Chem. Soc.* **1918,** 40, 1361-1403.

38. Olivier, J. P., Modeling Physical Adsorption on Porous and Nonporous Solids Using Density Functional Theory. *J. Porous Mat.* **1995,** 2, 9-17.

39. Dalla Fontana, G.; Fiore, G. L.; Battezzati, L., Thermodynamics of the Au49Ag5.5Pd2.3Cu26.9Si16.3 glass-forming alloy. *J. Non-Cryst. Solids* **2013,** 382, 95-98.

40. Myers, A. L.; Prausnitz, J. M., Thermodynamics of mixed-gas adsorption. *AIChe Journal* **1965,** 11, 121-127.

41. Simon, C. M.; Smit, B.; Haranczyk, M., pyIAST: Ideal adsorbed solution theory (IAST) Python package. *Computer Phys. Commun.* **2016,** 200, 364-380.

42. Hoff, T. C.; Thilakaratne, R.; Gardner, D. W.; Brown, R. C.; Tessonnier, J. P., Thermal Stability of Aluminum-Rich ZSM-5 Zeolites and Consequences on Aromatization Reactions. *J. Phys. Chem. C* **2016,** 120, 20103-20113.

43. Petrovic, I.; Navrotsky, A.; Davis, M. E.; Zones, S. I., Thermochemical Study of The Stability of Frameworks in High-Silica Zeolites. *Chem. Mat.* **1993,** 5, 1805-1813.

44. Ungár, T.; Gubicza, J.; Ribárik, G.; Pantea, C.; Zerda, T. W., Microstructure of carbon blacks determined by X-ray diffraction profile analysis. *Carbon* **2002,** 40, 929-937.

45. Vitillo, J. G.; Bordiga, S., Increasing the Stability of Mg_2(dobpdc) Metal-Organic Framework in Air Through Solvent Removal. *Mater. Chem. Front.* **2017**, 10.1039/c6qm00220j.

46. Thommes, M.; Kaneko, K.; Neimark, A. V.; Olivier, J. P.; Rodriguez-Reinoso, F.; Rouquerol, J.; Sing, K. S. W., Physisorption of gases, with special reference to the evaluation of surface area and pore size distribution (IUPAC Technical Report). *Pure Appl. Chem.* **2015,** 87, 1051-1069.

47. Armandi, M.; Garrone, E.; Areán, C. O.; Bonelli, B., Thermodynamics of Carbon Dioxide Adsorption on the Protonic Zeolite H-ZSM-5. *ChemPhysChem* **2009,** 10, 3316-3319 and references therein.

48. Pazé, C.; Bordiga, S.; Lamberti, C.; Salvalaggio, M.; Zecchina, A.; Bellussi, G., Acidic Properties of H−β Zeolite As Probed by Bases with Proton Affinity in the 118−204 kcal mol^{-1}: A FTIR Investigation. *J. Phys. Chem. B* **1997,** 101, 4740-4751.

49. Weiland, R. H.; Dingman, J. C.; Cronin, D. B., Heat capacity of aqueous monoethanolamine, diethanolamine, N-methyldiethanolamine, and N-methyldiethanolamine-based blends with carbon dioxide. *J. Chem. Eng. Data* **1997,** 42, 1004-1006.

50. Mu, B.; Walton, K. S., Thermal Analysis and Heat Capacity Study of Metal-Organic Frameworks. *J. Phys. Chem. C* **2011,** 115, 22748-22754.

51. Qiu, L. Y.; Laws, P. A.; Zhan, B. Z.; White, M. A., Thermodynamic investigations of zeolites NaX and NaY. *Can. J. Chem.-Rev. Can. Chim.* **2006,** 84, 134-139.

52. Qiu, L. Y.; Murashov, V.; White, M. A., Zeolite 4A: heat capacity and thermodynamic properties. *Solid State Sci.* **2000,** 2, 841-846.

53. Silva, G. G.; Musumeci, A. W.; Gomes, A. P.; Liu, J. W.; Waclawik, E. R.; George, G. A.; Frost, R. L.; Pimenta, M. A., Characterization of commercial double-walled carbon nanotube material: composition, structure, and heat capacity. *J. Mater. Sci.* **2009,** 44, 3498-3503.

54. Dunne, J. A.; Rao, M.; Sircar, S.; Gorte, R. J.; Myers, A. L., Calorimetric heats of adsorption and adsorption isotherms .2. O_2, N_2, Ar, CO_2, CH_4, C_2H_6, and SF_6 on NaX, H-ZSM-5, and Na-ZSM-5 zeolites. *Langmuir* **1996,** 12, 5896-5904.

55. Canivet, J.; Fateeva, A.; Guo, Y. M.; Coasne, B.; Farrusseng, D., Water adsorption in MOFs: fundamentals and applications. *Chem. Soc. Rev.* **2014,** 43, 5594-5617.

56. Ohlin, L.; Bazin, P.; Thibault-Starzyk, F.; Hedlund, J.; Grahn, M., Adsorption of CO_2, CH_4, and H_2O in Zeolite ZSM-5 Studied Using In Situ ATR-FTIR Spectroscopy. *J. Phys. Chem. C* **2013,** 117, 16972-16982.

57. Masala, A.; Vitillo, J. V.; Mondino, G.; Grande, C. A.; Blom, R.; Manzoli, M.; Marshall, M.; Bordiga, S., CO_2 capture in dry and wet conditions in UTSA-16 metal organic framework. *ACS Appl. Mater. Interf.* **2016**.

58. Newsome, D.; Gunawan, S.; Baron, G.; Denayer, J.; Coppens, M. O., Adsorption of CO_2 and N_2 in Na-ZSM-5: effects of Na+ and Al content studied by Grand Canonical Monte Carlo simulations and experiments. *Adsorpt.-J. Int. Adsorpt. Soc.* **2013,** 20, 157-171.

59. Arean, C. O.; Manoilova, O. V.; Palomino, G. T.; Delgado, M. R.; Tsyganenko, A. A.; Bonelli, B.; Garrone, E., Variable-temperature infrared spectroscopy: An access to adsorption thermodynamics of weakly interacting systems. *Phys. Chem. Chem. Phys.* **2002,** 4, 5713-5715.

60. Delgado, M. R.; Area, C. O., Thermodynamics of nitrogen adsorption on the zeolite H-FER. *Appl. Surf. Sci.* **2007,** 253, 5705-5708.

61. Hussein, M. A.; Abu-Zied, B. M.; Asiri, A. M., Preparation, characterization, and electrical properties of ZSM-5/PEG composite particles. *Polymer Comp.* **2014,** 35, 1160-1168.

Insert Table of Contents Graphic and Synopsis Here

Carbon capture materials: from the lab to materials design. The inclusion of H-ZSM-5 in a conductive carbon/zeolite monolith, suitable for Electric Swing Adsorption, showed decidedly improved performances with respect to the pure zeolite in term of capacity and hydrophobility.